IEEE Journal on Exploratory Solid-State Computational Devices and Circuits

Received 14 September 2019; revised 8 November 2019 and 2 December 2019; accepted 17 December 2019.
Date of publication 23 December 2019; date of current version 6 February 2020.

Digital Object Identifier 10.1109/JXCDC.2019.2961333

Materials Relevant to Realizing a Field-Effect Transistor Based on Spin–Orbit Torques

PHILLIP DANG[1], ZEXUAN ZHANG[2], JOSEPH CASAMENTO[3], XIANG LI[2], JASHAN SINGHAL[2], DARRELL G. SCHLOM[3,4], DANIEL C. RALPH[4,5], HUILI GRACE XING[2,3,4] (Senior Member, IEEE), and DEBDEEP JENA[2,3,4] (Senior Member, IEEE)

[1]School of Applied and Engineering Physics, Cornell University, Ithaca, NY 14853-0001 USA
[2]School of Electrical and Computer Engineering, Cornell University, Ithaca, NY 14853-0001 USA
[3]Department of Materials Science and Engineering, Cornell University, Ithaca, NY 14853-0001 USA
[4]Kavli Institute at Cornell for Nanoscale Science, Cornell University, Ithaca, NY 14853-0001 USA
[5]Department of Physics, Cornell University, Ithaca, NY 14853-0001 USA

CORRESPONDING AUTHOR: P. DANG (pd382@cornell.edu)

This work was supported in part by the National Science Foundation under Grant E2CDA 1740286 and Grant NewLAW EFRI 1741694 and in part by the Semiconductor Research Corporation under Grant nCORE task 2758. The work of Phillip Dang was supported by the National Science Foundation Graduate Research Fellowship under Grant DGE-1650441.

ABSTRACT Spin–orbit torque (SOT) is a promising mechanism for writing magnetic memories, while field-effect transistors (FETs) are the gold-standard device for logic operation. The spin–orbit torque field-effect transistor (SOTFET) is a proposed device that couples an SOT-controlled ferromagnet to a semiconducting transistor channel via the transduction in a magnetoelectric multiferroic (MF). This allows the SOTFET to operate as both a memory and a logic device, but its realization depends on the choice of appropriate materials. In this report, we discuss and parametrize the types of materials that can lead to an SOTFET heterostructure.

INDEX TERMS Field-effect transistors (FETs), magnetic materials, magnetoelectrics, multiferroics (MFs), spin–orbit torques (SOTs), spintronics, topological insulators.

I. INTRODUCTION

ALTHOUGH charge-based memory has made rapid advances in recent years via the NAND Flash and its recent 3-D vertical incarnation, they fall short in comparison with magnetic memories in the metrics of reading/writing energies and durability [1], [2]. The competitiveness of modern magnetic memories began with the discovery of giant magnetoresistance (GMR) of magnetic multilayers in 1988 [3], which introduced a method to utilize the spin of an electron to detect the magnetization orientation of a ferromagnet (FM) and enabled an efficient reading mechanism [4]. In the following years, advances in WRITE operations for GMR-based memories were discovered via the experimental observations [5], [6] of theoretically predicted spin-transfer torque (STT) [7] and that of spin–orbit torque (SOT) [8]–[10]. Today, the STT and SOT mechanisms are under investigation because of the lower energy consumption they offer compared to previous GMR-based memories. More importantly, because of the fast READ/WRITE times achieved in STT and SOT switching, magnetic memories are no longer limited solely to permanent storage; they are currently being explored for their capacity for nonvolatile, infinite endurance, energy-efficient, high-density magnetoresistive random access memories (MRAM) [11], [12].

Despite paving the way for high-density magnetic memories, the GMR and tunneling magnetoresistance (TMR) mechanisms produce a limited change in resistance between the distinct memory states of the magnetic layers resulting in longer READ times, higher READ energies, and potential READ errors in MRAM. By comparison, the change in resistance between the ON and OFF states of a semiconductor (SC) field-effect transistor (FET) is much larger, by several orders of magnitude; a magnetic memory could benefit significantly if had access to the large change in resistance exhibited by a SC. The large change in resistance not only increases the speed, energy efficiency, and reliability of reading magnetic memories but also opens the possibility of using magnetic memory devices in logic circuits, which require the large ON/OFF ratios offered by FETs. This could result in new architectures, such as processing in memory, which would significantly improve computational speed as a whole. One way to achieve this device benefit would be to exploit the newly developed family of multiferroics (MFs)—materials that are simultaneously magnetically ordered and

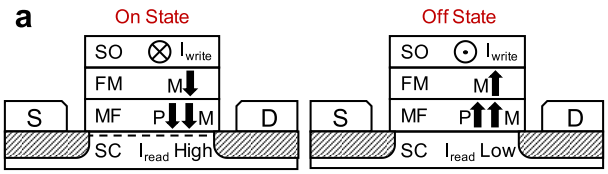

b

Material Type	Examples
Spin-Orbit Material (SO)	Bi_2Se_3, $Bi_{1-x}Sb_x$, Pt
Ferro/Ferrimagnet (FM)	Mn_4N, $Mn_{1-x}Ga_x$, $CoFe_2O_4$, $NiFe_2O_4$, $Y_3Fe_5O_{12}$
Multiferroic (MF)	$BiFeO_3$, $LuFeO_3$, $LuFeO_3/LuFe_2O_4$
Semiconductor (SC)	GaN, $BaSnO_3$, $MoSe_2$, Si

FIGURE 1. (a) Cartoon of SOTFET device for potential ON and OFF states. The arrows represent possible directions for magnetization (*M*) and electrical polarization (*P*). (b) Table of possible materials for implementation in the SOTFET.

ferroelectric—to sense the change in spin orientations from an SOT-ferromagnetic layer using exchange coupling to its magnetization on one side and transmit this signal through its electric polarization to a SC channel on the other. For this to happen, the magnetic order parameter should be coupled to the ferroelectric order parameter, which is the defining feature of a magnetoelectric MF material. Such a device is called the spin–orbit torque field-effect transistor (SOTFET). The SOTFET was recently proposed and analyzed by Li *et al.* [13], and its device and circuit implications were analyzed in [14]. In this article, we focus on the choices of materials that are desirable to realize the SOTFET and their present level of maturity.

II. SPIN–ORBIT TORQUE FIELD-EFFECT TRANSISTOR

The SOTFET consists of a semiconducting channel and a MF/FM/spin–orbit (SO) material gate stack. Fig. 1(a) shows a cartoon of the SOTFET and possible current, magnetization, and electrical polarization directions that would constitute the "ON" and "OFF" states of the transistor. We note that the actual directions of these vectors in a fully realized device could be different, depending on the ultimate choice of materials. Fig. 1(b) shows potential material choices for each layer of the SOTFET. From the top of the SOTFET gate stack to the channel, the SOTFET operates by using SOT to switch a ferromagnetic layer that is coupled to a magnetoelectric MF. When the direction of the spontaneous magnetization of the magnetoelectric MF is switched, the direction of its spontaneous electrical polarization is also deterministically switched. This change in polarization induces a change in electric field in the semiconducting channel that enhances or depletes the number of carriers in the semiconducting channel.

A. SPIN–ORBIT TORQUES

Magnetic memory has typically been based on the switching of the magnetic orientation of an FM and presents a nonvolatile and high-endurance form of information storage. In order to electrically detect the magnetic orientation of the FM, spin valves and magnetic tunnel junctions, based on GMR and TMR, have been widely researched. In these devices, a change in resistance up to ~600% [15] can occur when the magnetization of an FM is switched. STT is a phenomenon where nanoscale magnets can be switched by transferring the spin angular momentum of electrons from a spin-polarized current and the maximum angular momentum transferred by one electron in $\hbar/2$ [11]. SOT takes this idea of transferring spin angular momentum but utilizes a pure spin current generated within an SO material [12]. For example, when a charge current flows in the SO material shown in Fig. 1(a) and (b), it can generate a transverse-flowing spin current that can transfer nonequilibrium spin angular momentum to an adjacent FM. Each electron in the current flowing adjacent to the FM in an SOT device can transfer angular momentum several times, leading to a more efficient magnetic switch than in STT [12]. The SOTFET uses SOT as the switching mechanism, as illustrated in Fig. 1(a), but presents an alternative device structure to GMR- and TMR-based devices for the readout.

B. FERROMAGNET/FERROELECTRIC COUPLING

The SOTFET requires that the switching of an FM by SOT results in the deterministic switching of the spontaneous electrical polarization in a MF. In a magnetoelectric MF, the electrical polarization and magnetization are strongly coupled. For sufficient coupling between ferromagnetism and ferroelectricity and a sufficiently low energy barrier for switching the electrical polarization, it is expected that switching the spontaneous magnetization of the MF will deterministically switch the spontaneous electrical polarization of the MF. Furthermore, the magnetization of the ferromagnetic layer must be exchange-coupled to that of the MF layer. Such exchange coupling has been demonstrated most notably in a $BiFeO_3$–$Co_{0.9}Fe_{0.1}$ heterostructure with electric field control of magnetism [16], but the converse effect, which would enable the operation of the SOTFET, has not been demonstrated yet in this material. This is maybe due to the trend in MFs, the interactions that govern ferroelectricity are much larger in magnitude than those that govern magnetic ordering [17].

C. GATING OF THE FIELD-EFFECT TRANSISTOR

In an FET, an electric field applied through a voltage on the gate determines the density of charge carriers that conduct current in the semiconducting channel. In the SOTFET, the electrical polarization of the MF supplies the electric field required to gate the transistor. In the ideal situation, the change in electric field when the MF switches would be sufficient to switch the FET from its ON state to its OFF state, causing a large change in the SC channel resistance. This ON/OFF current ratio of the FET is determined by: 1) properties of the SC, such as the bandgap, carrier density, and carrier mobility and 2) the extent to which carrier concentration can be controlled by the electric field produced by the MF, which is determined by net polarization-charge

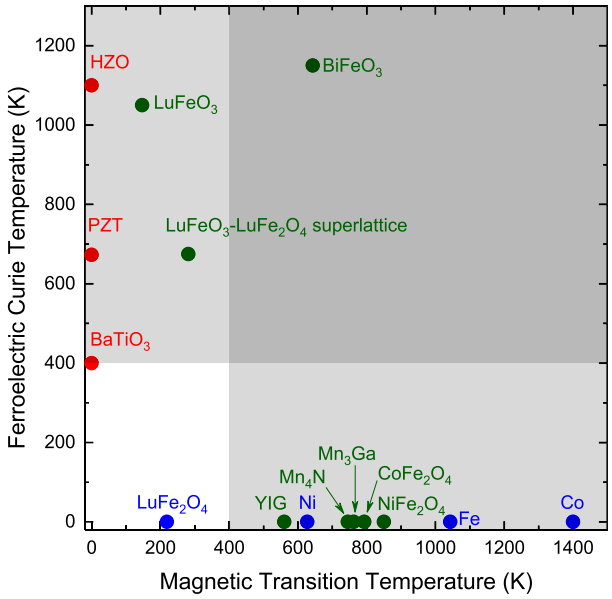

FIGURE 2. Neel and Curie Temperatures of ferroelectrics [18]–[20] (red), FMs [21] (blue), and ferrimagnets [21]–[27] (green). Shaded regions represent transition temperatures above 400 K, which are desirable for applications.

density, interface density of states, and electrostatic design of the channel (e.g., doping, layer thickness, geometry, etc.). The desired property for SOTFET operation is when the saturation polarization of the MF is comparable to the ON-state mobile charge sheet density in the semiconducting channel, which is typically in the 10^{12}–10^{13}/cm^2 regime and corresponds to a charge of $<2\ \mu$C/cm^2.

III. SEMICONDUCTORS AND MULTIFERROICS

The SC material desirable for the SOTFET should be able to intrinsically exhibit a large ON/OFF ratio of the conducting channel in response to the field effect and possess a high carrier mobility to reduce ohmic losses. That by itself is achievable in a large range of SCs for which FETs exist. The SOTFET, however, needs the field effect in the SC to be via the switchable electric polarization of a MF layer with which it is intimately integrated. The MF layer should ideally have a sufficient band offset with the SC band of interest and should be of a sufficient energy bandgap to avoid electrical shorting or ambipolar injection. Because of the limited choices of suitable MFs, the choice of SCs for the device is driven by their potential for integration with the suitable MF.

Magnetoelectric MFs are a class of materials that couple ferroic order parameters, namely, ferromagnetism and ferroelectricity. For many electronic device applications, including the SOTFET, this coupling should persist above room temperature. This is shown in the shaded gray box in Fig. 2 as magnetic and ferroelectric transition temperatures should ideally be above 400 K. Magnetic order generally decreases as temperature increases due to thermal fluctuations; similarly, ferroelectrics undergo charge order fluctuations or phase transitions that give rise to a paraelectric state at higher temperatures. For these reasons, as well as the complexity of interactions that govern magnetoelectric coupling, it is difficult to obtain room temperature or near-room temperature magnetoelectric MF materials. Only two magnetoelectric MFs have been demonstrated to deterministically switch near room temperature: $BiFeO_3$ [28] and $LuFeO_3/LuFe_2O_4$ superlattices [21]. Of these two, $BiFeO_3$ is the most widely studied as $BiFeO_3$ has the advantage of being thermodynamically stable, whereas $LuFeO_3/LuFe_2O_4$ superlattices are new artificial materials that are just beginning to be studied [29]. The family of relevant MFs is expected to expand in the future.

It is feasible to integrate layered, 2-D SCs on top of the MF as well, instead of growing the MF on a SC. This geometry is an "inverted" SOTFET when compared to Fig. 1. Although 2-D or layered SCs in principle can be mechanically integrated with the MF in a facile manner, the control of the chemical and electronic properties of the MF/2-D SC interface will determine its actual usefulness in the SOTFET. Since this usefulness is currently unknown, however, we limit our discussion of compatible SCs to 3-D SCs with promising compatibility with $BiFeO_3$ and $LuFeO_3/LuFe_2O_4$ superlattices.

A. MULTIFERROIC $BiFeO_3$

$BiFeO_3$ has primarily been grown epitaxially on insulating or metallic substrates to form capacitor structures for studying its MF properties. Early efforts to integrate $BiFeO_3$ with the wide-bandgap SC GaN resulted in a (0001)||(0001) epitaxial relationship, but required the use of $SrTiO_3$ and TiO_2 buffer layers [30]. From the point of view of epitaxial growth, the oxide SC $BaSnO_3$ provides the possibility of a high-mobility channel that is structurally matched with $BiFeO_3$. $BiFeO_3$ and $BaSnO_3$ are chemical compatible (both are oxides) and share the same crystal structure, both are perovskites. Importantly, $BaSnO_3$ is the highest electron mobility oxide perovskite known to date, with bulk room-temperature mobility exceeding 300 cm^2/V·s [31]. This is because unlike perovskites such as $SrTiO_3$ where the localized d-orbitals of the Ti atom form the conduction band, the high mobility of $BaSnO_3$ derives from the delocalized s-orbitals of the Sn atoms. Coupled with the large bandgap ($\sim$3 eV) [32], and the potential to sustain large electric fields, it is an attractive SC substrate for integration with $BiFeO_3$. Nevertheless, its band offsets with $BiFeO_3$ remain unexplored to date. Since the bandgap of $BiFeO_3$ (Eg $\sim$ 2.7 eV) [33] is only slightly smaller than that of $BaSnO_3$, it is important that the band offset be measured. It may be necessary to use a wider bandgap interlayers, for example, thin layers in which Sr is alloyed with $BaSnO_3$ as the alloy $(Ba_xSr_{1-x})SnO_3$.

B. MULTIFERROIC $LuFeO_3$ AND $LuFeO_3/LuFe_2O_4$ SUPERLATTICES

The main ingredient of the magnetoelectric MF $LuFeO_3/LuFe_2O_4$ superlattices [21] is $LuFeO_3$. At room temperature, it is ferroelectric and on cooling below 147 K becomes also MF [34]. By integrating $LuFeO_3$ into the $LuFeO_3$–$LuFe_2O_4$ superlattice structure, the magnetic transition temperature

raises to approximately 281 K. The $LuFeO_3$ polymorph of interest is hexagonal and metastable. There is also reason to believe that hexagonal $LuFeO_3$ may offer deterministic switching between **P** and **M** in its MF state [35]. By contrast, the stable polymorph of $LuFeO_3$ is centrosymmetric thus neither ferroelectric nor MF. The desired metastable polymorph of $LuFeO_3$ has been grown primarily on YSZ (111) substrates [36]. Nonetheless, hexagonal GaN or AlN substrates with *c*-plane orientation provide the correct symmetry matching [37]. There is a significant lattice mismatch, however, which would lead to defect formation in the $LuFeO_3$. The energy bandgap of $LuFeO_3$ is also rather small (~1 eV) [38], which implies a low chance of the desired large band offset to the underlying SC channel, e.g., GaN or AlN; this band offset has not yet been measured. Nevertheless, the nitride SC platforms offer a choice of mature and tested heterostructure platforms such as Al(Ga)N/GaN heterostructures, in which the current blocking is achievable by the wider bandgap interlayer. Hexagonal $LuFeO_3$ and its MF variants (including, for example, $LuFeO_3/LuFe_2O_4$ superlattices) must be grown on GaN under conditions that do not chemically modify (or oxidize) the GaN or intervening Al(Ga)N layers.

C. POLARIZATION AND MAGNETIZATION IN MULTIFERROICS

The MF behavior of $BiFeO_3$ is partially governed by the stereochemically active lone pair electrons in the Bi 6s orbital and their interaction with spins from the magnetic Fe atoms. The MF behavior of $LuFeO_3$—$LuFe_2O_4$ superlattices is partially governed by a trimer distortion (e.g., a physical rumpling of the $LuO_{1.5}$ layer involving a 2-up, 1-down positioning of Lu atoms) [35], which interacts with the spin moments of the neighboring iron ions. The difference in mechanisms causes the ferroelectric and magnetic transition temperatures to be largely different in each material. Accordingly, the strength of the magnetic and electrical-dipole moments is different for each. For SOT devices, it may be suitable to have a SC channel carrier concentration similar to the charge concentration arising from the spontaneous polarization in the MF material. For this reason, $LuFeO_3$ and $LuFeO_3$–$LuFe_2O_4$ superlattices are attractive, as well as La-substituted $BiFeO_3$ ($La_xBi_{1-x}FeO_3$), which reduces the spontaneous polarization compared to unsubstituted $BiFeO_3$ [39]. In theory, an SOT structure could be realized with only the magnetism from the MF, but the relatively weak canted moments of $BiFeO_3$ and $LuFeO_3$–$LuFe_2O_4$ superlattices on the order of 0.05 μB/formula unit may necessitate coupling with a magnetic material with a larger moment. This may aid in switching the electrical polarization by switching the magnetic moment of the MF material.

Fig. 3 shows the saturation electrical polarization P_s versus saturation magnetization M_s for MF materials and includes ferroelectric and ferromagnetic materials for comparison. The theoretical model of the SOTFET [13] suggests that switching a MF's electrical polarization by first switching its magnetization is facilitated when the polarization is reduced

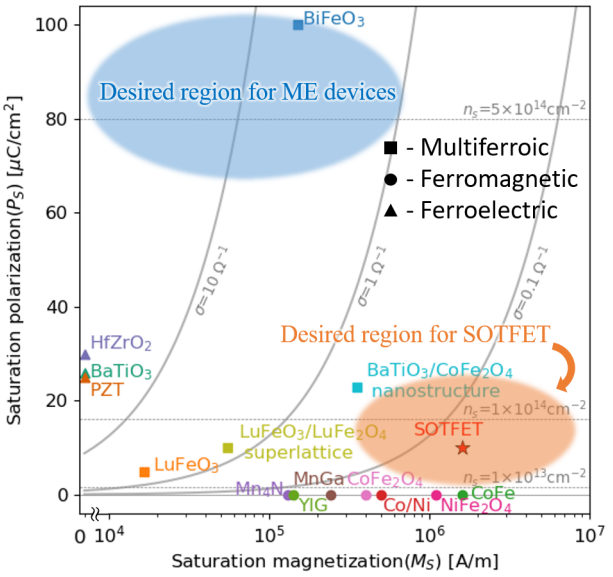

FIGURE 3. Polarization and magnetization of various ferroelectrics [40], [41] (triangles), FMs [29], [34], [42]–[47] (circles), and MFs [16]–[21], [34], [41], [48], [49] (squares). The solid gray curves represent fixed magnetoelectric transconductance, given by $\sigma = P_S/(\mu_0 M_S)$. The red star indicates the parameters used in [13] to theoretically demonstrate MF switching in an SOTFET.

and/or magnetization is increased (to enable strong exchange coupling to the magnetic layer). Therefore, we compare the relative strengths of polarization and magnetization in a MF by introducing a parameter $\sigma = P_s/(\mu_0 M_s)$, which has units of conductance despite no conduction happening within the MF. Fig. 3 utilizes σ, shown by the gray curves, as a figure of merit where low σ for a given magnetoelectric coupling energy is desired for the MF in an SOTFET. We note, however, that a more appropriate figure of merit must be a more specific quantification of magnetoelectric coupling energy that measures how easily the polarization of the MF can be driven by its magnetization. Nonetheless, the qualitative trend suggested in [13] supports our aim for low σ, and it can be used as a rule of thumb when engineering MF properties for the SOTFET. In Fig. 3, we imply that a region with low σ is beneficial for the SOTFET where magnetization is switched first, while a region with high σ is advantageous for magnetoelectric devices that switch polarization first. This would necessitate efforts to increase magnetization and exchange coupling, such as epitaxially stabilizing a hidden ground state of a frustrated ferrimagnet like $LuFe_2O_4$ [21], [29] and/or decrease polarization, such as by substituting La or other rare-earth ions into $BiFeO_3$ [39], [50], [51]. Decreasing polarization in the MF remains a priority because the expected polarization needed to control the semiconducting channel is on the order of 1 $\mu C/cm^2$, which is lower than most ferroelectrics and MFs, as shown in Fig. 3.

IV. FERRO/FERRIMAGNETS

For energy-efficient switching of a ferro/ferrimagnet using STT or SOT, ferro/ferrimagnets with perpendicular mag-

netic anisotropy (PMA) are generally favored for scaling. This is because PMA magnets require lower switching currents than in-plane anisotropic magnets for a given energy barrier for switching [52]. While lowering the energy barrier leads to lower switching currents, practical magnetic memory applications require energy barriers greater than $40\,k_BT$ so that retention time against thermal agitation is at least 10 years [52]. Therefore, we limit our discussion of ferro/ferrimagnetic materials to only those that have been demonstrated to have PMA. However, we note that in-plane magnetized magnets have been shown to couple to $BiFeO_3$ [16], indicating that SOTFETs can be realized with magnetic materials that do not exhibit PMA.

The zero-temperature critical switching current of PMA magnets under single-domain assumption can be written as $J^{\mathrm{SH}}_{C,\mathrm{perp}} = (2e/\hbar)(M_s t_F/\theta_{\mathrm{SH}})((H_{K,\mathrm{eff}}/2) - (H_x/\sqrt{2}))$, where $H_{K,\mathrm{eff}}$ is the effective anisotropy field representing the strength of the magnetic anisotropy, H_x is an in-plane external magnetic field, M_s is the saturation magnetization, t_F is the thickness of the magnet, and θ_{SH} is the spin Hall angle of an adjacent SO material [53]. Fig. 4 shows the anisotropy field and saturation magnetization for several magnets scaled down to 1 nm thicknesses. The gray dashed lines show the critical switching current, calculated using the above equation, for several PMA magnets of 1 nm thickness, with the heavy metal Pt or the topological insulator BiSb as the SOT layer in the limit of negligible external in-plane assist field, which gives an upper bound for the switching current. The numbers in this plot are based on the anisotropy fields and saturation magnetizations of these materials.

In real cases, SOT switching may proceed through domain wall motion instead of the coherent reversal of a single domain, as has been observed by magneto-optical Kerr effect (MOKE) microscopy in W/CoFeB/MgO heterostructures [62]. SOT switching can also be thermally excited. Therefore, the dashed lines in Fig. 4 are the upper bounds of critical switching currents. For an SOTFET where the ferro/ferrimagnet and MF magnetizations are strongly coupled, magnets with higher saturation magnetization may be advantageous because they raise the effective magnetization of the MF, lowering its effective σ and facilitating the switching of its polarization. However, magnets with higher saturation magnetization are also more difficult to switch by SOT. The conflicting requirements indicate that the saturation magnetization of the magnet should be neither too high, nor too low for use in the SOTFET.

On the other hand, ferro/ferrimagnets with a lower anisotropy field have smaller energy barriers for switching. However, if the anisotropy field is too small, the magnet is thermally unstable. Therefore, the optimal ferro/ferrimagnets in Fig. 4 fall in an intermediate region for integration in the SOTFET. This parameter space must be further explored, however, given the range of competing effects. It is important to note that the critical switching current shown in Fig. 4 is assumed to flow in the SO layer only, not the ferro/ferrimagnetic layer. Current shunting through metallic

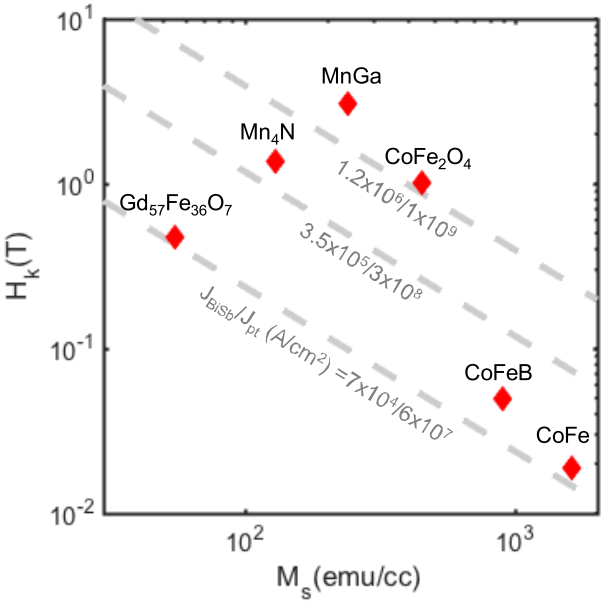

FIGURE 4. Anisotropy field and saturation magnetization for various PMA magnets [16], [34], [54]–[61]. The gray dashed lines represent calculated and fixed critical switching currents through Pt and BiSb.

ferro/ferrimagnets increases the actual total current required for SOT switching. From this point of view, insulating magnets, most of which are ferrimagnets such as yttrium iron garnet (YIG), $CoFe_2O_4$, and $NiFe_2O_4$, are quite promising for energy efficient SOT devices. Furthermore, insulating magnets may aid the MF as a gate dielectric in the SOTFET if the MF layer has too small of a band gap and/or is too electrically leaky.

V. SPIN–ORBIT MATERIALS

The SO materials work in conjunction with the ferromagnetic materials to determine the efficiency of magnetic switching by SOT. While properties of the ferromagnetic and MF layers determine the energy barrier required to switch magnetization, the properties of the SO layer determine how much energy can be used to switch the magnet for a given current. Hence, we desire an SO material that can transfer the most spin angular momentum to the FM for a fixed amount of input voltage. A useful metric to quantify this efficiency is the spin Hall conductivity (SHC), which is the product of spin Hall angle and electrical conductivity. The spin Hall angle is given by $\theta_{\mathrm{SH}} = 2e/\hbar(J_s/J_c)$, where J_s is the spin current and J_c is the charge current. In essence, the spin Hall angle evaluates how much spin angular momentum can be generated per unit of charge current density. Higher spin Hall angles are desired. High electronic conductivity in the SO layer is also desired in order to minimize current shunting into the FM if the FM is also electrically conductive. Fig. 5 shows the spin Hall angle and electronic conductivity for several potential SO materials. The gray dashed lines represent fixed SHCs, and the higher the SHC (the closer to the top-right corner of Fig. 5), the more desirable the SO material.

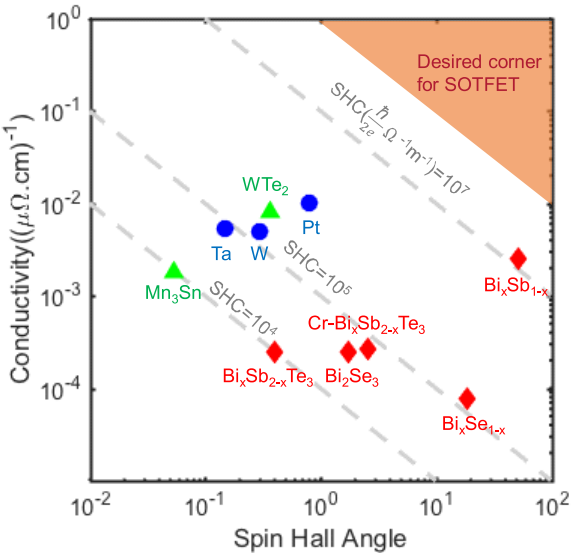

FIGURE 5. Conductivity versus spin Hall angle for SO materials. Blue circles are heavy metals [61], [63], [64], red diamonds are topological insulators [43], [65]–[69], and green triangles are topological semimetals [70], [71]. The gray lines represent fixed SHC, which is the product of spin Hall angle and conductivity.

The most promising SO materials, thus far, have mainly been heavy metals or topological insulators. The high nuclear charge of the atoms in heavy metals results in large SO coupling, leading to efficient charge-to-spin conversion. Heavy metals are also highly electrically conductive. Topological insulators are electrically insulating in the bulk but have conductive surface bands. The spins of electrons that occupy the surface bands are locked to their momentum. This spin-momentum locking leads to very efficient charge-to-spin conversion. On the other hand, most of the charge current and spin-polarization is confined to the surfaces, leading to low electronic conductivity of topological insulators [68], [71]. Materials with both large spin Hall angle and high electronic conductivity, which fall in the top right corner of Fig. 5, are, therefore, highly desired for most efficient SOT switching in general and for the SOTFET in particular.

Generally, heavy metals have higher electronic conductivity, while topological insulators have higher spin Hall angles. To date, the highest SHC measured at room temperature was for BiSb, a conductive topological insulator. It exhibited a giant spin Hall angle with electronic conductivity comparable to a heavy metal [43]. As alternatives to heavy metals and topological insulators, Dirac and Weyl topological semimetals have recently been proposed as SO materials [72]. Dirac and Weyl topological semimetals are new states of topological quantum matter with a linear dispersion at the Dirac or Weyl points. Very recently, it has been found that there exists very large fieldlike torque at low temperature [72] as well as out-of-plane antidamping torque through control of crystal symmetry in the semimetal WTe_2 [73], which offers probability of realizing deterministic SOT switching without the need for in-plane assisting magnetic fields. Thus, Fig. 5 offers a range of materials choices for the SO layer for the SOTFET. Compatibility with the underlying FM/MF/SC stack will determine which are practical.

VI. EPITAXIAL GROWTH

While we have discussed the materials parameters that are desirable for each material type in the SOTFET, we also must consider how these materials can be compatibly integrated into a single structure. Several techniques may be used for the fabrication of the SOTFET, but epitaxy holds several potential advantages in the efficacy of each SOTFET material layer. High-quality commercial SC technology is epitaxially grown on SC substrates, and the high degree of structural integrity of the crystals of epitaxial MFs assists in retaining their desired properties. Therefore, epitaxial growth will likely be required for the SC and MF layers in the SOTFET. Furthermore, the most efficient room temperature SOT switching to date had been demonstrated on an epitaxial structure [43], suggesting that it is important to explore and consider the epitaxial growth, ideally all in-situ, of the entire SOTFET structure to prove the feasibility of the device.

In epitaxial growth of thin films, it is desirable to generate smooth, single-crystalline films with low densities of defects such as dislocations, stacking faults, vacancies, and so on. One way to aid this is to utilize a substrate or template layer with the same or a very similar lattice constant and similar lattice symmetry as the desired film. This allows for a film to be grown in a very low strain state, which can prohibit the emergence of defects in the film that would act to relax the strain in the film. To this end, Fig. 6 plots the in-plane lattice constants of candidate SOTFET materials, as well as their energy band gaps. Energy band alignment is also important to consider since we want the MF (and the ferro/ferrimagnetic layer if insulating) to act as a gate dielectric and the SO layer (and the ferro/ferrimagnetic layer if conductive) to act as a gate metal. Lattice matching of (001) $BiFeO_3$-based and (0001) $LuFeO_3$-based SOTFETs is shown via the dashed vertical lines in Fig. 6, indicating the possibility of epitaxially integrating several families of materials from topological insulators to SCs.

By considering lattice constants, we can also utilize epitaxial strain to modify the material properties of each layer in the SOTFET. An example of epitaxial strain and symmetry-sensitive material properties is that $CoFe_2O_4$, when grown on a hexagonal substrate, will adopt the (111) orientation to have proper symmetry matching, and when grown on a cubic substrate with (001) orientation, $CoFe_2O_4$ tends to adopt the (001) orientation and exhibit PMA [84]. When tensile strained, $CoFe_2O_4$ exhibits out-of-plane anisotropy and when compressively strained displays in-plane anisotropy [85]. Accordingly, material properties are tunable through epitaxial engineering.

VII. CONCLUSION

SOTFET-based structures are posed to yield a promising combination of SOT phenomena with field-effect control of electrons in SCs. This is expected to enable novel devices and

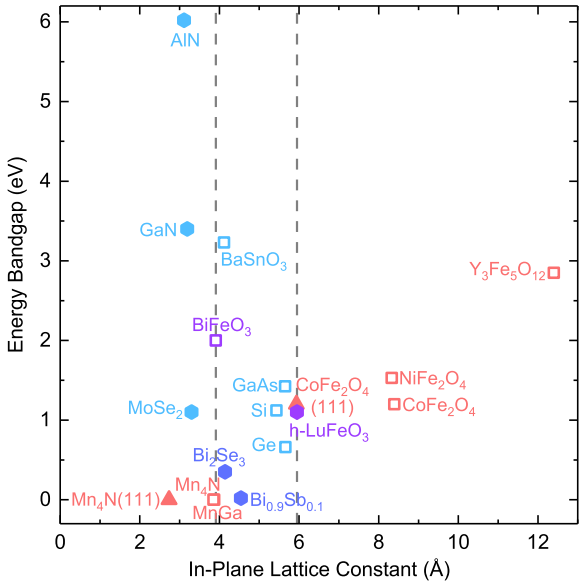

FIGURE 6. Lattice constants and bandgaps for SCs [74]–[76] (teal), MFs [33], [38] (purple), FMs [77]–[81] (orange), and topological insulators [82], [83] (blue). Hexagons represent hexagonal crystals, hollow squares represent cubic crystals, and triangles represent cubic crystals grown in the (111) direction. Materials with unlisted growth face planes are in the (001) orientation for the cubic crystals and in the (0001) orientation for the hexagonal crystals. The gray dotted lines are to guide the eyes along the lattice matching for SOTFETs based on $BiFeO_3$ and h-$LuFeO_3$.

architectures with combined memory and logic functionality. As high-quality advanced materials such as topological insulators, ferrimagnetic insulators, and magnetoelectric MFs continue to be uncovered via epitaxial engineering, the rich physics that govern these phenomena will likely soon be elucidated as well.

REFERENCES

[1] R. Bishnoi, M. Ebrahimi, F. Oboril, and M. B. Tahoori, "Architectural aspects in design and analysis of SOT-based memories," in *Proc. 19th Asia South Pacific Design Automat. Conf. (ASP-DAC)*, Jan. 2014, pp. 700–707.

[2] A. D. Kent and D. C. Worledge, "A new spin on magnetic memories," *Nature Nanotechnol.*, vol. 10, no. 3, pp. 187–191, 2015.

[3] M. N. Baibich *et al.*, "Giant magnetoresistance of (001)Fe/(001)Cr magnetic superlattices," *Phys. Rev. Lett.*, vol. 61, no. 21, pp. 2472–2475, 1988.

[4] A. Fert, "Nobel lecture: Origin, development, and future of spintronics," *Rev. Mod. Phys.*, vol. 80, no. 4, pp. 1517–1530, 2008.

[5] E. B. Myers, D. C. Ralph, J. A. Katine, R. N. Louie, and R. A. Buhrman, "Current-induced switching of domains in magnetic multilayer devices," *Science*, vol. 285, no. 5429, pp. 867–870, Aug. 1999.

[6] J. A. Katine, F. J. Albert, R. A. Buhrman, E. B. Myers, and D. C. Ralph, "Current-driven magnetization reversal and spin-wave excitations in Co/Cu/Co pillars," *Phys. Rev. Lett.*, vol. 84, no. 14, pp. 3149–3152, 2000.

[7] J. C. Slonczewski, "Conductance and exchange coupling of two ferromagnets separated by a tunneling barrier," *Phys. Rev. B, Condens. Matter*, vol. 39, pp. 6995–7002, Apr. 1989.

[8] A. Manchon and S. Zhang, "Theory of spin torque due to spin-orbit coupling," *Phys. Rev. B, Condens. Matter*, vol. 79, no. 9, Mar. 2009, Art. no. 094422.

[9] A. Chernyshov, M. Overby, X. Liu, J. K. Furdyna, Y. Lyanda-Geller, and L. P. Rokhinson, "Evidence for reversible control of magnetization in a ferromagnetic material by means of spin-orbit magnetic field," *Nature Phys.*, vol. 5, no. 9, pp. 656–659, Sep. 2009.

[10] I. M. Miron *et al.*, "Current-driven spin torque induced by the Rashba effect in a ferromagnetic metal layer," *Nature Mater.*, vol. 9, no. 3, pp. 230–234, 2010.

[11] D. C. Ralph and M. D. Stiles, "Spin transfer torques," *J. Magn. Magn. Mater.*, vol. 320, no. 7, pp. 1190–1216, 2008.

[12] P. Gambardella and I. M. Miron, "Current-induced spin-orbit torques," *Philos. Trans. Royal Soc. A, Math., Phys. Eng. Sci.*, vol. 369, no. 1948, pp. 3175–3197, Aug. 2011.

[13] X. Li *et al.*, "Spin-orbit-torque field Eect transistor (SOTFET): A new magnetoelectric memory," 2019, *arXiv 1909.08133*. [Online]. Available: https://arxiv.org/abs/1909.08133

[14] O. Afuye *et al.*, "Modeling and circuit design of associative memories with spin orbit torque FETs," *IEEE J. Explor. Solid-State Comput. Devices Circuits*, to be published, doi: 10.1109/JXCDC.2019.2952394.

[15] S. Ikeda *et al.*, "Tunnel magnetoresistance of 604% at 300 K by suppression of Ta diffusion in Co Fe B/ Mg O/Co Fe B pseudo-spin-valves annealed at high temperature," *Appl. Phys. Lett.*, vol. 93, no. 8, pp. 1–4, 2008.

[16] J. T. Heron *et al.*, "Electric-field-induced magnetization reversal in a ferromagnet-multiferroic heterostructure," *Phys. Rev. Lett.*, vol. 107, no. 21, 2011, Art. no. 217202.

[17] C. Lu, M. Wu, L. Lin, and J.-M. Liu, "Single-phase multiferroics: New materials, phenomena, and physics," *Nature Sci. Rev.*, vol. 6, no. 4, pp. 653–668, Jul. 2019.

[18] K.-I. Sakayori *et al.*, "Curie temperature of $BaTiO_3$," *Jpn. J. Appl. Phys.*, vol. 34, no. 9B, pp. 5443–5445, Sep. 1995.

[19] C.-C. Chung, "Microstructural evolution in lead zirconate titanate (PZT) piezoelectric ceramics," Ph.D. dissertation, Dept. Mater. Sci. Eng., North Carolina State Univ., Raleigh, NC, USA, 2014.

[20] J. Lyu, I. Fina, R. Solanas, J. Fontcuberta, and F. Sanchez, "Growth' window of ferroelectric epitaxial $Hf_{0.5}Zr_{0.5}O_2$ thin films," *ACS Appl. Electron. Mater.*, vol. 1, no. 2, pp. 220–228, Feb. 2019.

[21] J. A. Mundy *et al.*, "Atomically engineered ferroic layers yield a room-temperature magnetoelectric multiferroic," *Nature*, vol. 537, no. 7621, pp. 523–527, 2016.

[22] P. Hansen, J. Schuldt, and W. Tolksdorf, "Anisotropy and magnetostriction of iridium-substituted yttrium iron garnet," *Phys. Rev. B, Condens. Matter*, vol. 8, no. 9, pp. 4274–4287, Nov. 1973.

[23] G. Catalan and J. F. Scott, "Physics and applications of bismuth ferrite," *Adv. Mater.*, vol. 21, pp. 2463–2485, Jun. 2009.

[24] W. J. Takei, R. R. Heikes, and G. Shirane, "Magnetic structure of Mn_4N-type compounds," *Phys. Rev.*, vol. 125, no. 6, pp. 1893–1897, Mar. 1962.

[25] J. Winterlik *et al.*, "Structural, electronic, and magnetic properties of tetragonal $Mn_{3-x}Ga$: Experiments and," *Phys. Rev. B, Condens. Matter*, vol. 77, no. 5, Feb. 2008, Art. no. 054406.

[26] C. Zhou *et al.*, "The phase diagram and exotic magnetostrictive behaviors in spinel oxide $Co(Fe_{1-x}Al_x)_2O_4$ system," *Materials*, vol. 12, no. 10, p. 1685, May 2019.

[27] U. Luders, M. Bibes, J.-F. Bobo, M. Cantoni, R. Bertacco, and J. Fontcuberta, "Enhanced magnetic moment and conductive behavior in $NiFe_2O_4$ spinel," *Phys. Rev. B, Condens. Matter*, vol. 71, no. 13, p. 134419, Apr. 2005.

[28] J. T. Heron *et al.*, "Deterministic switching of ferromagnetism at room temperature using an electric field," *Nature*, vol. 516, no. 7531, pp. 370–373, Dec. 2014.

[29] R. Ramesh and D. G. Schlom, "Creating emergent phenomena in oxide superlattices," *Nature Rev. Mater.*, vol. 4, no. 4, pp. 257–268, Mar. 2019.

[30] W. Tian *et al.*, "Epitaxial integration of (0001) $BiFeO_3$ with (0001) GaN," *Appl. Phys. Lett.*, vol. 90, no. 17, Apr. 2007, Art. no. 172908.

[31] W.-J. Lee *et al.*, "Transparent perovskite barium stannate with high electron mobility and thermal stability," *Annu. Rev. Mater. Res.*, vol. 47, no. 1, pp. 391–423, Jul. 2017.

[32] H. J. Kim *et al.*, "Physical properties of transparent perovskite oxides (Ba,La)SnO_3 with high electrical mobility at room temperature," *Phys. Rev. B, Condens. Matter*, vol. 86, no. 16, pp. 1–9, 2012.

[33] J. F. Ihlefeld *et al.*, "Optical band gap of $BiFeO_3$ grown by molecular-beam epitaxy," *Appl. Phys. Lett.*, vol. 92, no. 14, Apr. 2008, Art. no. 142908.

[34] J. A. Moyer *et al.*, "Intrinsic magnetic properties of hexagonal $LuFeO_3$ and the effects of nonstoichiometry," *APL Mater.*, vol. 2, no. 1, Jan. 2014, Art. no. 012106.

[35] H. Das, A. L. Wysocki, Y. Geng, W. Wu, and C. J. Fennie, "Bulk magnetoelectricity in the hexagonal manganites and ferrites," *Nature Commun.*, vol. 5, no. 1, p. 2998, May 2014.

[36] A. A. Bossak *et al.*, "XRD and HREM studies of epitaxially stabilized hexagonal orthoferrites $RFeO_3$ (R = EuLu)," *Chem. Mater.*, vol. 16, no. 9, pp. 1751–1755, May 2004.

[37] J. Casamento *et al.*, "MBE growth of epitaxial multiferroic hexagonal $LuFeO_3$ on GaN," unpublished.

[38] B. S. Holinsworth *et al.*, "Direct band gaps in multiferroic h -$LuFeO_3$," *Appl. Phys. Lett.*, vol. 106, no. 8, Feb. 2015, Art. no. 082902.

[39] Y. H. Chu *et al.*, "Low voltage performance of epitaxial $BiFeO_3$ films on Si substrates through lanthanum substitution," *Appl. Phys. Lett.*, vol. 92, no. 10, Mar. 2008, Art. no. 102909.

[40] S. Tiwari, *Nanoscale Device Physics: Science and Engineering Fundamentals*. London, U.K.: Oxford Univ. Press, 2017.

[41] J. Muller *et al.*, "Ferroelectricity in simple binary ZrO_2 and HfO_2," *Nano Lett.*, vol. 12, no. 8, pp. 4318–4323, Aug. 2012.

[42] Y. Yasutomi, K. Ito, T. Sanai, K. Toko, and T. Suemasu, "Perpendicular magnetic anisotropy of Mn_4N films on MgO(001) and $SrTiO_3$(001) substrates," *J. Appl. Phys.*, vol. 115, no. 17, pp. 10–13, 2014.

[43] N. H. D. Khang, Y. Ueda, and P. N. Hai, "A conductive topological insulator with large spin Hall effect for ultralow power spin-orbit torque switching," *Nature Mater.*, vol. 17, no. 9, pp. 808–813, Sep. 2018.

[44] C. Gatel, B. Warot-Fonrose, S. Matzen, and J.-B. Moussy, "Magnetism of $CoFe_2O_4$ ultrathin films on $MgAl_2O_4$ driven by epitaxial strain," *Appl. Phys. Lett.*, vol. 103, no. 9, Aug. 2013, Art. no. 092405.

[45] Y. Henry, S. Mangin, J. Cucchiara, J. A. Katine, and E. E. Fullerton, "Distortion of the Stoner-Wohlfarth astroid by a spin-polarized current," *Phys. Rev. B, Condens. Matter*, vol. 79, no. 21, Jun. 2009, Art. no. 214422.

[46] D. Y. Qiu, K. Ashraf, and S. Salahuddin, "Nature of magnetic domains in an exchange coupled $BiFeO_3$/CoFe heterostructure," *Appl. Phys. Lett.*, vol. 102, no. 11, Mar. 2013, Art. no. 112902.

[47] Y. Li *et al.*, "Giant anisotropy of Gilbert damping in epitaxial CoFe films," *Phys. Rev. Lett.*, vol. 122, no. 11, Mar. 2019, Art. no. 117203.

[48] W. Wang *et al.*, "Room-temperature multiferroic hexagonal $LuFeO_3$ films," *Phys. Rev. Lett.*, vol. 110, no. 23, Jun. 2013, Art. no. 237601.

[49] H. Zheng *et al.*, "Multiferroic $BaTiO_3$-$CoFe_2O_4$ Nanostructures," *Science*, vol. 303, no. 5658, pp. 661–663, Jan. 2004.

[50] S. K. Singh and H. Ishiwara, "Doping effect of rare-earth ions on electrical properties of $BiFeO_3$ thin films fabricated by chemical solution deposition," *Jpn. J. Appl. Phys.*, vol. 45, no. 4, pp. 3194–3197, 2006.

[51] O. E. González-Vázquez, J. C. Wojdeł, O. Diéguez, and J. Íñiguez, "First-principles investigation of the structural phases and enhanced response properties of the $BiFeO_3$-$LaFeO_3$ multiferroics," *Phys. Rev. B, Condens. Matter*, vol. 85, no. 6, Feb. 2012, Art. no. 064119.

[52] S. Mangin, D. Ravelosona, J. A. Katine, M. J. Carey, B. D. Terris, and E. E. Fullerton, "Current-induced magnetization reversal in nanopillars with perpendicular anisotropy," *Nature Mater.*, vol. 5, no. 3, pp. 210–215, 2006.

[53] K.-S. Lee, S.-W. Lee, B.-C. Min, and K.-J. Lee, "Threshold current for switching of a perpendicular magnetic layer induced by spin Hall effect," *Appl. Phys. Lett.*, vol. 102, no. 11, 2013, Art. no. 112410.

[54] T. Gushi *et al.*, "Mn4N ferrimagnetic thin films for sustainable spintronics," 2019, *arXiv:1901.06868*. [Online]. Available: https://arxiv.org/abs/1901.06868

[55] R. Ranjbar, K. Z. Suzuki, Y. Sasaki, L. Bainsla, and S. Mizukami, "Current-induced spin-orbit torque magnetization switching in a MnGa/Pt film with a perpendicular magnetic anisotropy," *Jpn. J. Appl. Phys.*, vol. 55, no. 12, 2016.

[56] M. H. Carvalho *et al.*, "Determination of the effective anisotropy constant of $CoFe_2O_4$ nanoparticles through the T-dependence of the coercive field," *J. Appl. Phys.*, vol. 119, no. 9, 2016, Art. no. 093909.

[57] F. Eskandari, S. B. Porter, M. Venkatesan, P. Kameli, K. Rode, and J. M. Coey, "Magnetization and anisotropy of cobalt ferrite thin films," *Phys. Rev. Mater.*, vol. 1, no. 7, pp. 1–34, 2017.

[58] S. Lee, J. Chung, X. Liu, J. K. Furdyna, and B. J. Kirby, "Ferromagnetic semiconductor GaMnAs," *Mater. Today*, vol. 12, no. 4, pp. 14–21, 2009.

[59] V. B. Naik, H. Meng, and R. Sbiaa, "Thick CoFeB with perpendicular magnetic anisotropy in CoFeB-MgO based magnetic tunnel junction," *AIP Adv.*, vol. 2, no. 4, 2012, Art. no. 042182.

[60] J. Cao *et al.*, "Spin orbit torques induced magnetization reversal through asymmetric domain wall propagation in Ta/CoFeB/MgO structures," *Sci. Rep.*, vol. 8, no. 1, pp. 1–9, 2018.

[61] L. Liu, O. J. Lee, T. J. Gudmundsen, D. C. Ralph, and R. A. Buhrman, "Current-induced switching of perpendicularly magnetized magnetic layers using spin torque from the spin Hall effect," *Phys. Rev. Lett.*, vol. 109, no. 9, pp. 1–5, 2012.

[62] X. Zhao *et al.*, "Ultra-efficient spinorbit torque induced magnetic switching in W/CoFeB/MgO structures," *Nanotechnology*, vol. 30, no. 33, Aug. 2019, Art. no. 335707.

[63] L. Liu, C.-F. Pai, Y. Li, H. W. Tseng, D. C. Ralph, and R. A. Buhrman, "Spin-torque switching with the giant spin Hall effect of tantalum," *Science*, vol. 336, no. 6081, pp. 555–558, May 2012.

[64] C.-F. Pai, L. Liu, Y. Li, H. W. Tseng, D. C. Ralph, and R. A. Buhrman, "Spin transfer torque devices utilizing the giant spin Hall effect of tungsten," *Appl. Phys. Lett.*, vol. 101, no. 12, pp. 1–5, 2012.

[65] A. R. Mellnik *et al.*, "Spin-transfer torque generated by a topological insulator," *Nature*, vol. 511, pp. 449–451, Jul. 2014.

[66] Y. Wang *et al.*, "Room temperature magnetization switching in topological insulator-ferromagnet heterostructures by spin-orbit torques," *Nature Commun.*, vol. 8, no. 1, pp. 6–11, 2017.

[67] J. Han, A. Richardella, S. Siddiqui, J. Finley, N. Samarth, and L. Liu, "Room-temperature spin-orbit torque switching induced by a topological insulator," *Phys. Rev. Lett.*, vol. 119, Aug. 2017, Art. no. 077702.

[68] M. DC *et al.*, "Room-temperature high spinorbit torque due to quantum confinement in sputtered BixSe(1-x) films," *Nature Mater.*, vol. 17, no. 9, pp. 800–807, Sep. 2018.

[69] H. Wang *et al.*, "Fermi level' dependent spin pumping from a magnetic insulator into a topological insulator," *Phys. Rev. Res.*, vol. 1, no. 1, Aug. 2019, Art. no. 012014.

[70] B. Zhao *et al.*, "Observation of spin hall effect in weyl semimetal WTe_2 at room temperature," Dec. 2018, *arXiv:1812.02113*. [Online]. Available: https://arxiv.org/abs/1812.02113

[71] P. K. Muduli *et al.*, "Evaluation of spin diffusion length and spin Hall angle of the antiferromagnetic Weyl semimetal Mn_3Sn," *Phys. Rev. B, Condens. Matter*, vol. 99, no. 18, pp. 1–9, 2019.

[72] P. Li *et al.*, "Spin-momentum locking and spin-orbit torques in magnetic nano-heterojunctions composed of Weyl semimetal WTe_2," *Nature Commun.*, vol. 9, no. 1, p. 3990, Dec. 2018.

[73] D. MacNeill, G. M. Stiehl, M. H. Guimaraes, R. A. Buhrman, J. Park, and D. C. Ralph, "Control of spin-orbit torques through crystal symmetry in WTe_2/ferromagnet bilayers," *Nature Phys.*, vol. 13, no. 3, pp. 300–305, 2017.

[74] *NSM Archive—Physical Properties of Semiconductors*. Accessed: Sep. 6, 2019. [Online]. Available: http://www.ioffe.ru/SVA/NSM/Semicond/

[75] B. Hadjarab, A. Bouguelia, and M. Trari, "Optical and transport properties of lanthanum-doped stannate BaSnO3," *J. Phys. D, Appl. Phys.*, vol. 40, no. 19, pp. 5833–5839, Oct. 2007.

[76] S. Vishwanath, P. Dang, and H. G. Xing, "Challenges and opportunities in molecular beam epitaxy growth of 2D crystals," in *Molecular Beam Epitaxy*. Amsterdam, The Netherlands: Elsevier, 2018, pp. 443–485.

[77] H. Yang, H. Al-Brithen, E. Trifan, D. C. Ingram, and A. R. Smith, "Crystalline phase and orientation control of manganese nitride grown on MgO(001) by molecular beam epitaxy," *J. Appl. Phys.*, vol. 91, no. 3, pp. 1053–1059, 2002.

[78] X. Jia, K. Liu, K. Xia, and G. E. Bauer, "Spin transfer torque on magnetic insulators," *Europhys. Lett.*, vol. 96, no. 1, pp. 1–6, 2011.

[79] B. S. Holinsworth *et al.*, "Chemical tuning of the optical band gap in spinel ferrites: $CoFe_2O_4$ vs $NiFe_2O_4$," *Appl. Phys. Lett.*, vol. 103, no. 8, Aug. 2013, Art. no. 082406.

[80] M. Meinert and G. Reiss, "Electronic structure and optical band gap determination of NiFe2O4," *J. Phys., Condens. Matter*, vol. 26, no. 11, Mar. 2014, Art. no. 115503.

[81] A.-O. Mandru *et al.*, "Structure and magnetism in Ga-rich MnGa/GaN thin films and unexpected giant perpendicular anisotropy in the ultra-thin film limit," *Appl. Surf. Sci.*, vol. 367, pp. 312–319, Mar. 2016.

[82] A. L. Jain, "Temperature dependence of the electrical properties of bismuth-antimony alloys," *Phys. Rev.*, vol. 114, no. 6, pp. 1518–1528, Jun. 1959.

[83] N. Bansal *et al.*, "Epitaxial growth of topological insulator Bi_2Se_3 film on Si(111) with atomically sharp interface," *Thin Solid Films*, vol. 520, no. 1, pp. 224–229, Oct. 2011.

[84] H. Yanagihara, K. Uwabo, M. Minagawa, E. Kita, and N. Hirota, "Perpendicular magnetic anisotropy in $CoFe_2O_4$(001) films epitaxially grown on MgO(001)," *J. Appl. Phys.*, vol. 109, no. 7, Apr. 2011, Art. no. 07C122.

[85] X. S. Gao *et al.*, "Switching of magnetic anisotropy in epitaxial $CoFe_2O_4$ thin films induced by $SrRuO_3$ buffer layer," *J. Phys. D, Appl. Phys.*, vol. 42, no. 17, Sep. 2009, Art. no. 175006.